



Power Electronic Systems
Laboratory

© 2014 IEEE

Proceedings of the International Power Electronics Conference - ECCE Asia (IPEC 2014), Hiroshima, Japan, May 18-21, 2014

Topology Evaluation of Slotless Bearingless Motors with Toroidal Windings

D. Steinert,
T. Nussbaumer,
J. W. Kolar

This material is published in order to provide access to research results of the Power Electronic Systems Laboratory / D-ITET / ETH Zurich. Internal or personal use of this material is permitted. However, permission to reprint/republish this material for advertising or promotional purposes or for creating new collective works for resale or redistribution must be obtained from the copyright holder. By choosing to view this document, you agree to all provisions of the copyright laws protecting it.



Eidgenössische Technische Hochschule Zürich
Swiss Federal Institute of Technology Zurich

Topology Evaluation of Slotless Bearingless Motors with Toroidal Windings

Daniel Steinert

Power Electronic Systems Laboratory
ETH Zurich, Switzerland
steinert@lem.ee.ethz.ch

Thomas Nussbaumer

Levitronix GmbH
Zurich, Switzerland
nussbaumer@levitronix.com

Johann W. Kolar

Power Electronic Systems Laboratory
ETH Zurich, Switzerland
kolar@lem.ee.ethz.ch

Abstract— In this paper, different winding and magnet topologies are analyzed and compared for a slotless bearingless disk drive with toroidal windings. Basis of the studies is a six phase motor with a diametrically magnetized one-pole-pair rotor. Due to the absence of mechanical bearings, the motor is suitable for applications with high purity and special chemical demands. Its slotless design results in low losses even at high rotational speeds. To improve the operational behavior of the rotor in different applications, the influence of higher pole pair numbers on the passive bearing stiffness is examined. Possible winding configurations for these rotors are presented and evaluated for their bearing and motor performance. Based on the results, a further prototype was built and is presented in this paper.

Keywords— Active magnetic bearing, bearingless motor, high speed drive, slotless motor

I. INTRODUCTION

In a bearingless slice motor, developed by Schoeb and Barletta [1], a disk- or ring-shaped rotor is spatially suspended and rotated without any mechanical contact. Due to the lack of lubrication and abrasion as well as the possibility to hermetically isolate rotor and stator from the environment, bearingless motors are used for example in semiconductor manufacturing [2], chemical or biological industries [3], [4], medicine, or in high speed applications [5]. Furthermore, the disk topology results in an enhanced compactness due to its low axial length.

In the presented slotless bearingless motor concept a disk shaped rotor is levitated magnetically without mechanical contact in the middle of an annular stator (cf. Fig. 1). The coils, which are wound toroidally on the stator iron, can generate both bearing forces and drive torque. [6]–[8]

Due to the absence of mechanical contact between rotor and stator, mechanical bearings and shaft feed-throughs can be omitted. This allows for a hermetic encapsulation of rotor and stator, which results in high resistance against chemically aggressive fluids and gases and in increased lifetime compared to conventional motors. The absence of abrasion and lubrication enables operation in high purity applications.

However, magnetic bearings have a significantly lower bearing stiffness than mechanical ones, which limits the possible applications. In pumps and blowers for instance, axial and radial forces resulting from the differential pressure of the fluid act on the impeller. This means

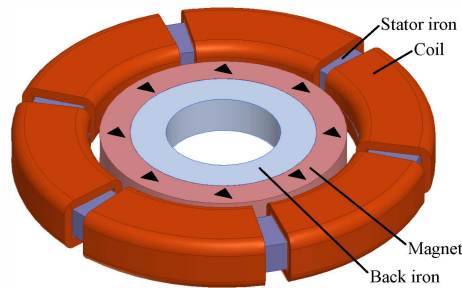


Fig. 1. Principle setup of a slotless bearingless disk drive with six coils and a diametrically magnetized permanent magnet rotor. The coils generate both, force and torque, simultaneously. A six phase inverter is necessary for operation.

possibly a considerable movement of the magnetically levitated rotor and limits the achievable pump, blower or turbine performance [9].

To improve both the passive bearing stiffness and the active bearing and motor performance of the bearingless motor, different rotor magnetizations, rotor pole pair numbers and winding configurations will be examined in this paper.

At first, the magnetic air gap field distributions for diametrical, radial and Halbach magnetization of the rotor are evaluated. The influence of the pole pair number on the passive bearing stiffnesses and on the drive and bearing performance is shown.

As only specific winding configurations are capable of generating torque and force independently for a given rotor magnetization, we derive the criteria for developing suitable configurations. The winding concepts differ with regard to the coil number and the interconnection of the coils. Additionally, it has to be distinguished between combined coils, which generate force and torque with one set of coils, and separate coils for motor and bearing. By 2D and 3D finite element simulations, selected winding configurations are compared regarding their bearing and motor capabilities, as well as passive stiffnesses and losses. Additionally, the influence of the pole pair number on the iron losses is estimated. At the end, a prototype with two pole pair rotor will be presented and compared to the existing one pole pair motor.

II. WORKING PRINCIPLE OF THE SLOTLESS BEARINGLESS DISK DRIVE

In [6] the authors present the detailed working principles as well as simulation and test results of the bearingless slotless disk drive with six coils and a

diametrically magnetized one-pole-pair rotor. The presented prototype is the basis for the topology evaluation in this paper.

The disk type bearingless motor is passively stable in tilting and axial direction and has to be actively controlled in radial direction. The magnetic field in the magnetic gap, as is shown in Fig. 2 for a one- and a two-pole-pair rotor, generates reluctance forces between the stator iron and the rotor. Therefore, a deflection in the axial z-direction will lead to a counteracting force

$$dF_z = -c_z \cdot dz \quad (1)$$

due to the axial stiffness constant c_z similarly to a spring constant. With this definition, a positive value of the stiffness leads to a stabilizing force.

Similarly, the tilting of the rotor results in a counteracting torque. At a rotor with pole pair number $p=1$ it has to be distinguished between rotation around the axis of magnetization (angle α) or perpendicular to it (angle β). The tilting stiffnesses c_α and c_β are then defined by

$$c_\alpha = -\frac{dT_\alpha}{d\alpha} \text{ and } c_\beta = -\frac{dT_\beta}{d\beta}. \quad (2)$$

When the rotor is displaced from its center position in radial direction, a radial force will act in the same direction. Therefore, the radial stiffnesses

$$c_d = -\frac{dF_x}{dx_d} \text{ and } c_q = -\frac{dF_y}{dx_q} \quad (3)$$

are destabilizing. Here, x_d means a displacement in the direction of the magnetization and x_q perpendicular to the magnetization.

A one-pole-pair rotor results in anisotropic radial and tilting stiffness. Deflection of the rotor in the direction of magnetization (d-axis) results in a higher attractive force than deflection perpendicular to the magnetization (q-axis). The same holds for the tilting stiffness. A rotation around the d-axis results in a lower torque than rotation around q-axis. This results in a broad resonance frequency range, as is shown in [10]. Rotors with higher pole pair numbers, however, show almost isotropic stiffnesses in all directions.

$$\begin{aligned} p = 1: & c_\alpha < c_\beta \text{ and } c_q < c_d \\ p \geq 2: & c_\alpha \approx c_\beta \text{ and } c_q \approx c_d \end{aligned} \quad (4)$$

To stabilize the passively unstable radial position, an actively controlled force has to be applied on the rotor. It

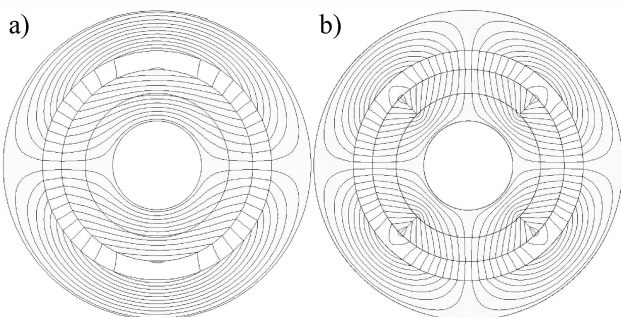


Fig. 2. Simulated magnetic field lines with a diametrically magnetized one-pole-pair rotor (a) and a two-pole-pair rotor with radial magnetization (b). The outer ring is the slotless stator, the rotor consists of the magnet ring and a backiron on its inner side. The coils of the motor are not shown here.

can be shown that the bearing force F_{bng} as well as the drive torque T

$$\vec{F}_{bng} = k_F \cdot \hat{I}_B \begin{pmatrix} \cos(\varphi_F) \vec{e}_x \\ \sin(\varphi_F) \vec{e}_y \end{pmatrix} \quad (5)$$

$$T = k_T \cdot \hat{I}_D \quad (6)$$

are proportional to the peak bearing current \hat{I}_B or drive current \hat{I}_D with the force coefficient k_F and the drive coefficient k_T . The force direction can be controlled by the phase shift φ_F between electrical rotor angle and bearing current.

III. EVALUATION OF PASSIVE BEARING PROPERTIES FOR DIFFERENT MAGNET CONFIGURATIONS

Depending on the application, considerably large magnetic gaps are necessary, for instance if a chemically resistant wall has to be inserted between rotor and stator. This drastically reduces the passive stiffnesses of the bearing, as shown in [7]. Therefore, a strong magnetic field in the air gap between magnet and stator iron is important. Moreover, the active force and torque generation depends especially on the fundamental wave of the flux density distribution in the air gap.

With 2D FE simulations, the magnetic field in the magnetic gap between rotor and stator is simulated. Fig. 3 shows the evaluated magnet configurations with one and two pole pairs, as well as the harmonic analysis of the magnetic field distribution in the middle of the magnetic gap.

For a rotor with one pole pair ($p = 1$), only the diametrical magnetization is of interest, as it yields the best results with a purely sinusoidal magnetic air gap field. However, as shown before, the stiffnesses are anisotropic leading to an unfavorable resonance behavior.

Going to higher pole pair numbers, different magnetization schemes are possible. The radial magnetization yields the highest flux density, however also higher harmonics in the field distribution. A back iron carries the flux at the inner side of the rotor and therefore enhances the flux density in the magnetic gap.

The Halbach magnetization has lower harmonics and does not need a back iron, but the fundamental wave is reduced by 18 %. The tangential distribution yields an even lower fundamental wave and higher harmonics and therefore promises the lowest performance.

With a fixed geometry (cf. Table I) 3D simulations have been conducted with different pole pair numbers and magnetization schemes. It shows that the highest passive stiffness values can be achieved with $p = 2$. The axial stiffness (cf. Fig. 4) increases by 39% and the mean tilting stiffness (cf. Fig. 5) increases by 37% with a radial magnetization compared to the diametrical magnetization. Furthermore, the tilting stiffnesses are isotropic for the $p \geq 2$ magnetizations. This means an increase of the minimal tilting stiffness by 300%, when changing the magnetization from one to two pole pairs.

When the space inside the hollow shaft rotor has to be used in the application, e.g. in axial blowers, the back iron can be omitted. This results in a weaker air gap field and in reduced stiffnesses. A radial magnetized two-pole-pair

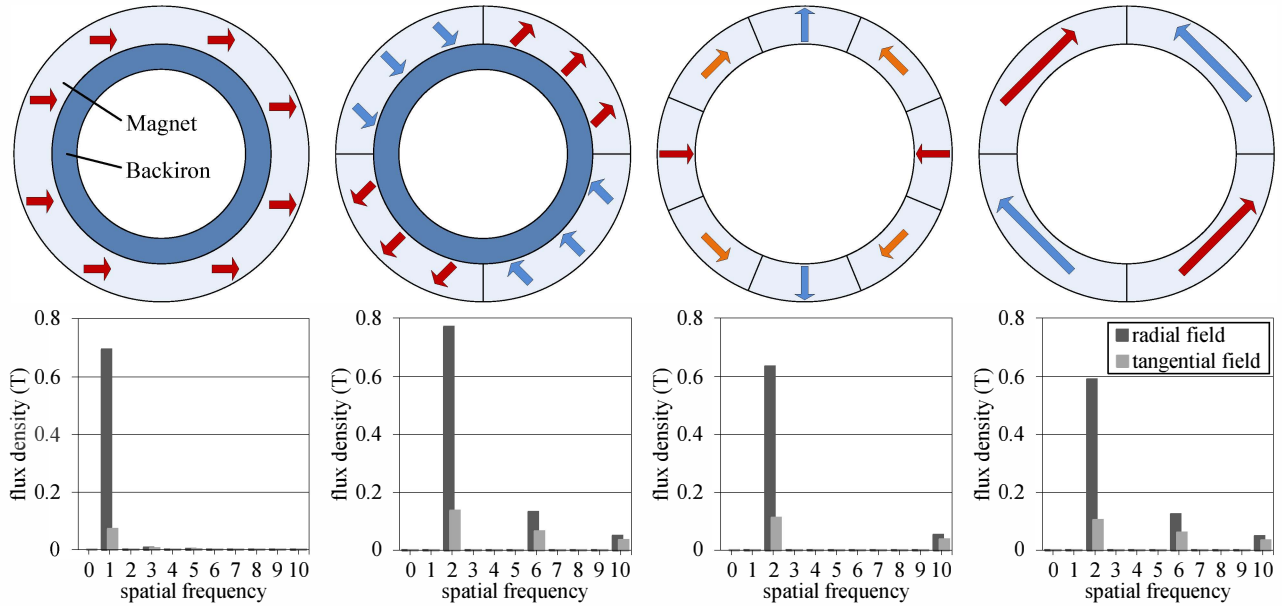


Fig. 3. Schematic drawing of the magnet configurations suitable for application in the bearingless disk motor (top) and FFT of the flux density distribution in the middle of the air gap between rotor magnet and stator iron (bottom). F.l.t.r: Diametrical magnetization (one pole pair), radial magnetization, Halbach magnetization and tangential magnetization (each two pole pairs).

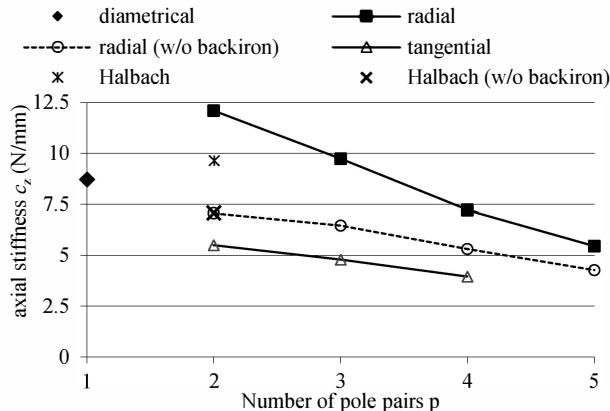


Fig. 4. Axial stiffness simulated with 3D FEM for different magnet configurations.

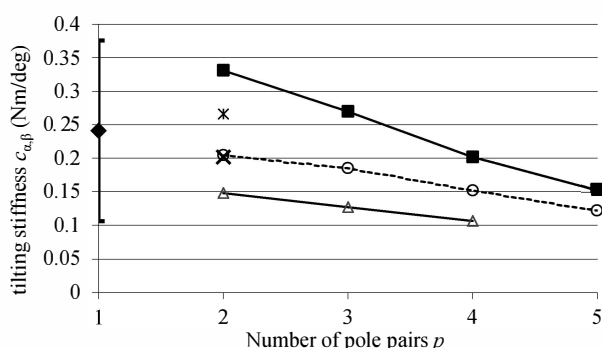


Fig. 5. Tilting stiffness simulated with 3d FEM for different magnet configurations. For the diametrical magnetization the mean value is given and the highest and lowest tilting stiffness is indicated.

TABLE I
GEOMETRY PARAMETERS OF THE EXAMINED TOPOLOGIES

Parameter	Value
outer magnet diameter	97 mm
outer stator diameter	156 mm
inner stator diameter	116 mm
magnetic gap	9.5 mm
magnet height	15 mm
stator height	12.5 mm

rotor without back iron shows about 40% lower stiffness. A Halbach magnetized rotor without back iron has nearly the same stiffnesses as a rotor with radial magnetization. Tangential magnetization always shows the weakest stiffnesses.

Summarizing, the highest passive bearing stiffnesses can be achieved with a radial magnetized rotor with two pole pairs. A further increase of the pole number reduces the stiffnesses. If a rotor without backiron shall be used, radial and Halbach magnetization are equal.

IV. WINDING CONCEPTS

To generate torque acting on the rotor, the stator coils have to generate a magnetic armature reaction field in the magnetic gap with a pole pair number

$$p_{\text{drv}} = p \quad (7)$$

that is equal to the pole pair number p of the rotor magnetic field. A force will be generated by a stator field with a pole pair number

$$p_{\text{bng}} = p \pm 1. \quad (8)$$

The bearing forces consist of reluctance and Lorentz forces that act in the same direction when the stator pole pair number is greater than the rotor field, otherwise both forces partially cancel each other out. [2]

Therefore, to achieve high bearing forces, a magnetic air gap field with $p_{\text{bng}} = p + 1$ has to be generated by the set of coils.

To derive a winding configuration that is capable of generating both torque and force independently, it has to be distinguished between combined coils and separated coils.

A. Winding criteria for combined coils

With combined coils, both torque and force are generated by the same set of coils. Because of the different pole numbers for bearing and drive, the winding scheme

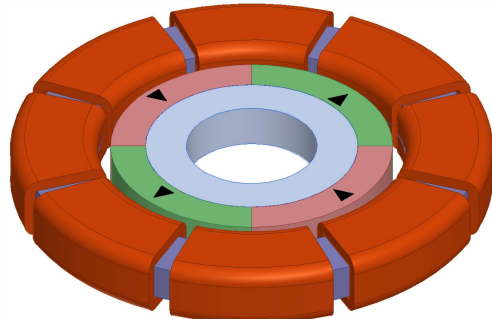


Fig. 6. Bearingless motor with a two-pole-pair rotor and eight combined coils for force and torque. An eight-phase inverter is necessary for operation.

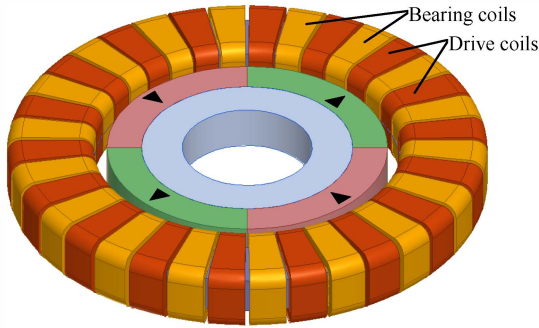


Fig. 7. Bearingless motor with a two-pole-pair rotor and 36 coils in total. Each 18 coils are either for bearing or motor operation. Motor and bearing operation can be done by two independent three-phase inverters.

contains no repetitive elements. This means that the number of phases m equals the number of coils N . However, one coil can be separated in two coils with reversed winding direction, which are connected in series, as it is proposed in [10]. This will have no direct effect on the feasibility of the winding configuration and is not examined in this paper.

To generate a field with a given pole pair number p , at least

$$N \geq 2 \cdot p \quad (9)$$

coils are necessary to avoid aliasing. Additionally, the number of phases divided by the pole pair number for the bearing field

$$\frac{m}{p_{\text{bng}}} \neq 1, 2, 4 \quad (10)$$

must not equal 1, 2 or 4. Otherwise, the phase shift between two phases would be a multiple of 90° and at times when one phase current is zero it wouldn't be possible to control both radial degrees of freedom. Therefore, there is one direction, where no force can be generated at a certain time and no stable bearing operation would be possible.

With the criteria in (9), (10) at least seven coils are necessary for a rotor with pole pair number $p = 2$. As eight coils can be connected in two star points, this configuration can be realized by a controller with eight half bridges and six current sensors (cf. Fig. 6).

B. Winding criteria for separated coils

With separated coils, the magnetic field for each bearing and motor operation is generated by an independent set of coils. Therefore, two independent

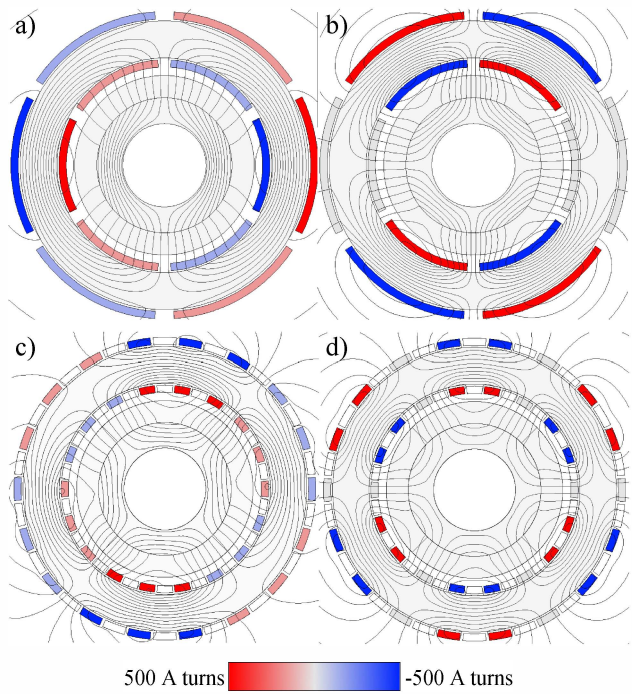


Fig. 8. Simulated armature reaction field due to the coil currents indicated by different shades of blue and red. The magnetic field of the rotor is not shown here. The upper figures show the six coil topology with combined coils with a drive current (a) that generates a one pole pair field, and a bearing current (b) with a two pole pair field. In the 2x18 coil topology, the drive currents generate a two-pole-pair field (c) and the bearing currents generate a three-pole pair field (d). Bearing and drive currents are combined in the six coil topology, and separated on different coil sets in the 2x18 coil topology.

inverters can be used. Then, the winding configuration consists of repetitive elements corresponding to the respective pole pair number of bearing and motor field.

For the bearing field, at least three phases per pole pair are necessary, as two degrees of freedom have to be controlled and two coils per pole pair would result in a phase shift of 90° as already explained.

To maintain manufacturability, the coil numbers for bearing and motor have to be the same. Therefore, winding configurations with nine coils or eighteen coils (cf. Fig. 7) each for bearing and motor are possible.

C. Simulation results of proposed topologies

For the four mentioned topologies, the armature reaction field caused by drive and bearing currents is simulated and analyzed by FFT analysis. Fig. 8 shows the field lines of the armature reaction field for the 6-coil-topologie and the 2x18-coil topology. Fig. 9 shows the FFT of the armature reaction field in the magnetic gap for all four topologies of interest.

At the 6-coil-topology, the drive current shows a field with solely one first harmonic, which corresponds to the first harmonic of the diametrical rotor and generates a torque according to (7). The bearing current generates a force on the rotor due to its second harmonic armature reaction field. The higher harmonics are of low amplitude and can be neglected.

For the 8-coil-topology, the second and sixth harmonic of the drive field fits very well to the diametrical rotor, which shows a similar spectrum. The force on the rotor is generated by the third and fifth harmonic of the bearing

field interacting with the second and sixth harmonic of the rotor field. The results are similar to the 2x18-coil topology, where bearing and drive coils are separated.

For the 2x9-coil topology, however, it can be seen that the drive field shows a fifth and seventh harmonic, which generate a force in combination with the sixth harmonic of the rotor field. Additionally, the bearing field has a sixth harmonic, which generates a torque. Therefore, force and torque are interconnected, which most likely will make the control of this topology more difficult.

Subsequently, the 8-coil-topology with combined windings and the 2x9- and 2x18-coil-topologies with separated windings have been simulated in 3D FE simulations and compared to the 6-coil topology with diametrical rotor. The results are shown in Table II. It shows that the three topologies with two-pole-pair rotor gain in force and torque compared to the 6-coil topology. The 2x18-coil topology is better in force generation than the 8-coil topology, but has lower torque output.

The simulation of the 2x9-coil topology confirmed the interconnection of bearing and drive. It shows, that a drive current generates a force corresponding to a bearing current with an amplitude of 25% of the drive current. Vice versa, the bearing current generates a torque ripple of 15.6% corresponding drive current. This interconnection might lead to instable behavior of the motor, if the control does not compensate this interconnection.

Summarizing, with the 8- and 2x18-coil topology, promising alternatives to the diametrical magnetized 6-coil topology are developed. The passive stiffnesses as well as the active bearing and drive performance exceed the values of the 6-coil topology. As the 2x18-coil topology shows the best bearing force performance, it was decided to build up a prototype of this new topology. This prototype is presented and compared to the 6-coil prototype in section VI.

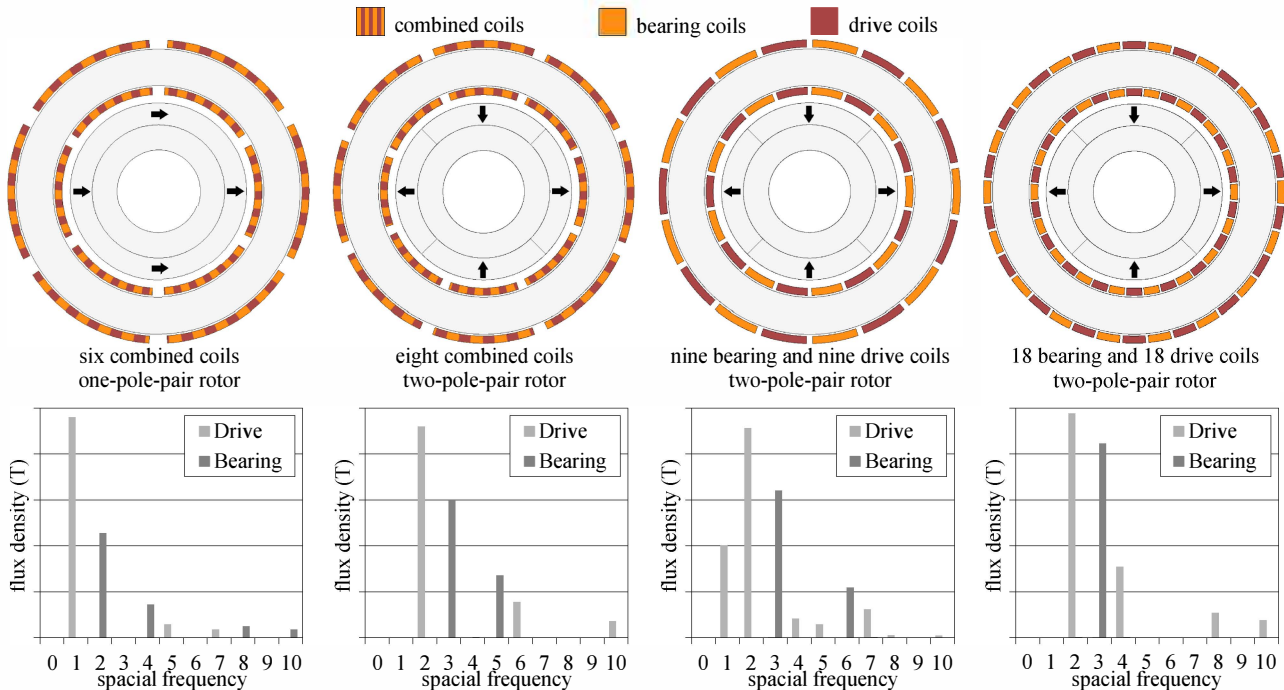


Fig. 9: Schematic drawing of the four evaluated winding topologies (top) and FFT analysis of the armature reaction field (without rotor field) generated by drive or bearing currents in the middle of the magnetic gap.

TABLE II
COMPARISON OF PROPOSED TOPOLOGIES WITH DIAMETRICAL AND RADIAL MAGNETIZED ROTOR

p	N	m	k_T ($\frac{\text{Nm}}{\text{A/mm}^2}$)	k_F ($\frac{\text{N}}{\text{A/mm}^2}$)	c_z ($\frac{\text{N}}{\text{mm}}$)	c_α ($\frac{\text{Nm}}{\text{deg}}$)	c_β ($\frac{\text{Nm}}{\text{deg}}$)
1	6	6	0.27	4.93	8.7	0.11	0.38
2	8	8	0.31	5.59	12.1	0.33	0.33
2	2x9	2x3	0.31	5.94	12.1	0.33	0.33
2	2x18	2x3	0.29	6.63	12.1	0.33	0.33

k_T ... Torque per peak current density in the coils

k_F ... Force per peak current density in the coils

c_z ... Axial stiffness

c_α ... Stiffness against tilting around d-axis

c_β ... Stiffness against tilting around q-axis

TABLE III
COMPARISON OF 36-COIL TOPOLOGY WITH DIFFERENT ROTOR MAGNETIZATIONS

Magnetization	Back iron	k_T ($\frac{\text{Nm}}{\text{A/mm}^2}$)	k_F ($\frac{\text{N}}{\text{A/mm}^2}$)	c_z ($\frac{\text{N}}{\text{mm}}$)	c_α ($\frac{\text{Nm}}{\text{deg}}$)
Radial	yes	0.29	6.63	12.1	0.33
Halbach	yes	0.26	6.08	9.7	0.27
Tangential	yes	0.29	6.63	12.1	0.33
Radial	no	0.21	4.85	7.1	0.20
Halbach	no	0.22	5.05	7.1	0.20
Tangential	no	0.22	4.32	5.5	0.15

V. LOSSES

In [6] it is shown, that the main losses of the slotless bearingless disk drive, especially at the proposed prototype, consist of iron losses in the stator. According to [11], these iron losses

$$P_{\text{Fe}} = P_{\text{Hy}} + P_{\text{Ed}} \quad (11)$$

can be separated into hysteresis losses P_{Hy} and eddy current losses P_{Ed} . The hysteresis losses

$$P_{\text{Hy}} = c_{\text{Hy}} \cdot f_{\text{el}} \cdot \hat{B}^{1.6} \cdot m_{\text{Fe}} \quad (12)$$

depend linearly on the electric frequency f_{el} , whereas the

eddy current losses

$$P_{\text{Ed}} = c_{\text{Ed}} \cdot f_{\text{el}}^2 \cdot \hat{B}^2 \cdot d_{\text{Fe}}^2 \cdot m_{\text{Fe}} \quad (13)$$

increase quadratically with the frequency. Both loss components are supposed to scale linearly with the mass of the stator iron m_{Fe} and also depend on the peak flux density \hat{B} in the stator. The coefficients c_{Ed} and c_{Hy} describe material properties.

Therefore, increasing the pole pair number of the rotor from $p = 1$ to $p = 2$ will double the electric frequency. Thus, the hysteresis losses will be twice as high whereas the eddy current losses will be even four times higher. Therefore, higher pole pair numbers are supposed to be less suitable for high speeds.

To better compare the losses of the two prototypes, which will be presented in the next section, we introduce two new coefficients $c_{n,1}$ and $c_{n,2}$ being the coefficients of a quadratic approximation of the motor losses according to the rotational speed and normalized to the stator iron mass. Therefore, the motor losses can be written as

$$P = c_{n,1} \cdot m_{\text{Fe}} \cdot n + c_{n,2} \cdot m_{\text{Fe}} \cdot n^2. \quad (14)$$

VI. TEST RESULTS

The first prototype ('prototype 1') with a diametrical magnetized one-pole-pair rotor and six combined coils has already been built and successfully tested (Fig. 10) [6]. Stable operation is possible for up to 20 000 rpm, which is the mechanical limit of the rotor.

Additionally, a second prototype ('prototype 2') with a two-pole-pair rotor and 2x18 separated coils for bearing and drive is built (cf. Fig. 11) and will now be compared to prototype 1. As higher iron losses are expected at the same rotational speed, prototype 2 was built with a significantly bigger rotor outer diameter, so that higher circumferential speeds can be achieved with lower rotational speeds.

While prototype 1 has a rotor diameter of 102 mm, the new prototype has a rotor size of 164.8 mm. The bigger size also enhances the manufacturability especially with the high number of coils that have to be placed on the stator of prototype 2. The geometrical details of both prototypes are compared in Table IV.

With prototype 2, rotational speeds of up to 12 000 r/min are reached [12]. This is the limit of mechanically safe operation. The prototype showed stable bearing behavior in standstill and during rotation. Rigid body resonances were observed between 1000-2000 r/min. Outside of this range, no resonances occurred. The



Fig. 10. Test setup of the slotless bearingless disk drive with six coils and diametrically magnetized rotor.

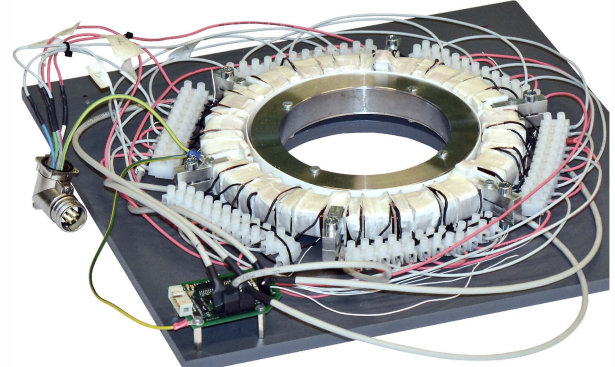


Fig. 11. Test setup of the slotless bearingless disk drive with 36 coils and a two pole pair, radial magnetized rotor.

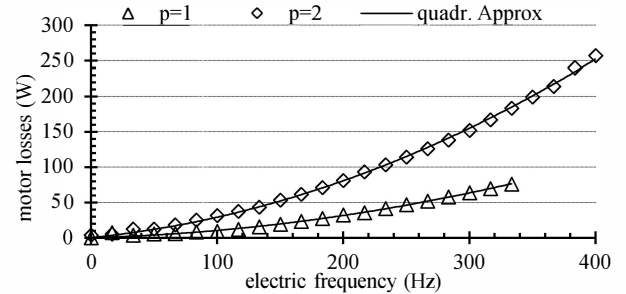


Fig. 12 Measured losses of the two prototypes shown for different electrical frequencies. The losses of prototype 2 are more than twice as high as prototype 1 at the same electrical frequency, although it rotates half as fast due to the two pole pairs.

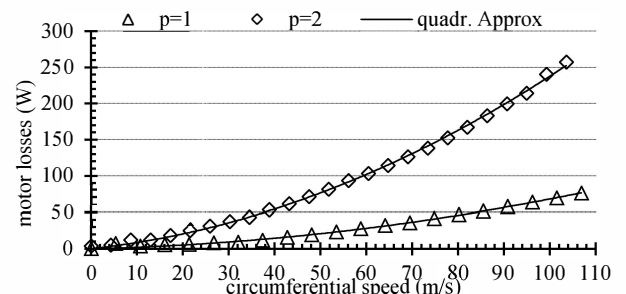


Fig. 13 Measured losses of the two prototypes shown for different circumferential speeds. As prototype 2 is bigger than prototype 1, it has a higher circumferential speed as the smaller prototype at the same rotational speed. The circumferential speed is important for the application like blowers or pumps.

TABLE V
COEFFICIENTS OF QUADRATIC APPROXIMATION
OF THE MEASURED NO LOAD LOSSES

	Prototype 1	Prototype 2	
c_{Hy}	0.0231	0.0553	(W Hz ⁻¹ kg ⁻¹ B ^{-1.6})
c_{Ed}	1501	2017	(W Hz ² kg ⁻¹ B ^{-2.3} m ⁻²)
$c_{n,1}$	$0.95 \cdot 10^{-3}$	$4.20 \cdot 10^{-3}$	(W rpm ⁻¹ kg ⁻¹)
$c_{n,2}$	$1.88 \cdot 10^{-7}$	$9.17 \cdot 10^{-7}$	(W rpm ⁻¹ kg ⁻¹)

separation of bearing and drive coils proved to be advantageous during implementation of drive and bearing, as the control of both three-phase current systems is independent. Additionally, the coils for bearing and drive could be adapted in size and number of turns to their respective function. It also can be demonstrated, that the stiffnesses of the two pole pair rotor are isotropic and significantly stronger than in prototype 1. Measurements of the axial stiffness fit nearly exactly to the simulated values.

The losses, however, proved to be even higher in prototype 2 than expected. In Fig. 12 the measured losses of both prototypes are plotted against the electric frequency. This means, that prototype 1 rotates twice as fast as prototype 2 at the same electric frequency. It can be seen that the losses in prototype 2 are more than two times higher at the same frequency. When plotting the losses against the circumferential speed (cf. Fig. 13), the losses are even worse compared to prototype 1. This is important for applications as blowers or pumps, where high circumferential speeds are necessary.

The measured losses can be approximated very well with the quadratic equations (11) and (14). The parameters are shown in Table V. The peak flux density in the stator of both prototypes was simulated and with the different mass of both stators, the coefficients are calculated. It shows, that the coefficients c_{Ed} and c_{Hd} are not constant for both prototypes as would be expected for material constants, which shows that other loss mechanisms are present. The quadratic coefficient is 34% higher in prototype 2, the linear loss coefficient is even 140% higher. However, the biggest loss component is the quadratic loss term. It is supposed, that other loss terms in addition to the iron losses (such as copper and air friction losses) cannot be completely neglected in the analysis. Additionally, the radially magnetized rotor in prototype 2 produces higher flux harmonics in the air gap field, which might also cause higher losses.

VII. CONCLUSION

Summarizing, it can be said that at disk type motors with sufficiently large outer diameter, a two-pole-pair rotor will lead to significantly higher passive bearing stiffnesses. Different coil topologies were proposed, which are possible with a two-pole-pair rotor. All topologies feature a higher number of coils, which leads to a bigger effort during manufacturing. A motor with 36 coils was built to demonstrate the feasibility of a two-pole-pair machine. It showed a very stable operational behavior and high isotropic stiffnesses. However, it showed also that the losses of a two-pole-pair rotor are much bigger than with a one-pole-pair rotor. Especially when high speeds are required, the one-pole-pair rotor might be chosen, whereas the two-pole-pair rotor is for applications with bigger demands on the passive stiffness.

REFERENCES

- [1] R. Schoeb and N. Barletta, "Principle and Application of a Bearingless Slice Motor," *JSME Int. J. Ser. C Mech. Syst. Mach. Elem. Manuf.*, vol. 40, no. 4, pp. 593–598, Dezember 1997.
- [2] F. Zürcher, T. Nussbaumer, and J. W. Kolar, "Motor Torque and Magnetic Levitation Force Generation in Bearingless Brushless Multipole Motors," *IEEEASME Trans. Mechatron.*, vol. 17, no. 6, pp. 1088–1097, Dec. 2012.
- [3] B. Warberger, R. Kaelin, T. Nussbaumer, and J. W. Kolar, "50-Nm/2500-W Bearingless Motor for High-Purity Pharmaceutical Mixing," *IEEE Trans. Ind. Electron.*, vol. 59, no. 5, pp. 2236–2247, May 2012.
- [4] T. Reichert, T. Nussbaumer, and J. W. Kolar, "Bearingless 300-W PMSM for Bioreactor Mixing," *IEEE Trans. Ind. Electron.*, vol. 59, no. 3, pp. 1376–1388, Mar. 2012.
- [5] S. Silber, J. Sloupenky, P. Dirnberger, M. Moravec, M. Reisinger, and W. Amrhein, "High Speed Drive for Textile Rotor Spinning Applications," *IEEE Trans. Ind. Electron.*, vol. Early Access Online, 2013.
- [6] D. Steinert, T. Nussbaumer, and J. Kolar, "Slotless Bearingless Disk Drive for High-Speed and High-Purity Applications," *IEEE Trans. Ind. Electron.*, vol. Early Access Online, 2014.
- [7] D. Steinert, T. Nussbaumer, and J. W. Kolar, "Concept of a 150 krpm Bearingless Slotless Disc Drive with Combined Windings," in *Proceedings of the IEEE International Electric Machines and Drives Conference (IEMDC 2013)*, Chicago, USA, 2013.
- [8] H. Mitterhofer, W. Gruber, and W. Amrhein, "On the High Speed Capacity of Bearingless Drives," *IEEE Trans. Ind. Electron.*, vol. 61, no. 6, pp. 3119–3126, Jun. 2014.
- [9] H. Mitterhofer, B. Mrak, and W. Amrhein, "Suitability investigation of a bearingless disk drive for micro turbine applications," in *2013 IEEE Energy Conversion Congress and Exposition (ECCE)*, 2013, pp. 2480–2485.
- [10] H. Mitterhofer, W. Amrhein, and H. Grabner, "Comparison of two- and four-pole rotors for a high speed bearingless drive," presented at the ISMB 2012, The 13th International Symposium on Magnetic Bearings, Arlington, USA, 2012.
- [11] M. T. Bartholet, T. Nussbaumer, S. Silber, and J. W. Kolar, "Comparative Evaluation of Polyphase Bearingless Slice Motors for Fluid-Handling Applications," *IEEE Trans. Ind. Appl.*, vol. 45, no. 5, pp. 1821–1830, Sep. 2009.
- [12] P. Peralta Fierro, "High Speed Slotless Bearingless Axial Blower," Master thesis, ETH Zurich, Zurich, 2014.